

## Light meson spectrum with $N_f = 2$ dynamical overlap fermions

---

JLQCD collaboration: J. Noaki<sup>\*a†</sup>, S. Aoki<sup>b</sup>, H. Fukaya<sup>c</sup>, S. Hashimoto<sup>a,d</sup>  
T. Kaneko<sup>a,d</sup>, H. Matsufuru<sup>a</sup>, T. Onogi<sup>e</sup>, E. Shintani<sup>a</sup>, N. Yamada<sup>a,d</sup>

<sup>a</sup> High Energy Accelerator Research Organization (KEK), Tsukuba 305-0801, Japan

<sup>b</sup> Graduate School of Pure and Applied Sciences, University of Tsukuba, Tsukuba 305-8571, Japan

<sup>c</sup> Theoretical Physics Laboratory, RIKEN, Wako 351-0198, Japan

<sup>d</sup> School of High Energy Accelerator Science, the Graduate University for Advanced Studies (Sokendai), Tsukuba 305-0801, Japan

<sup>e</sup> Yukawa Institute for Theoretical Physics, Kyoto University, Kyoto 606-8502, Japan

We present numerical simulation of QCD with two dynamical quark flavors described by the overlap fermion action on a  $16^3 \times 32 \times (0.12 \text{ fm})^4$  lattice. We calculate pseudo-scalar masses and decay constants and investigate their chiral properties. We test the consistency of our data with the two-loop chiral perturbation theory predictions, which should also be valid at finite lattice spacings because of the exact chiral symmetry, including the finite size effects.

*The XXV International Symposium on Lattice Field Theory*  
July 30 - August 4 2007  
Regensburg, Germany

---

\*Speaker.

†E-mail: noaki@post.kek.jp

## 1. Introduction

Thanks to the exact chiral symmetry, lattice simulation with the overlap fermions [1] provides a unique opportunity to approach low energy hadron physics. One of the major issues in this energy region is the consistency between QCD and chiral perturbation theory (ChPT). With the overlap fermion, the continuum ChPT can be applied without modification, that is not true with other fermion formulations that violate either chiral or flavor symmetry.

In this talk, we present two-flavor QCD simulation using the overlap fermion and the Iwasaki gauge action. On a  $16^3 \times 32$  lattice, we generate 10,000 trajectories [2, 3, 4, 5, 6] at six different sea quark masses. We explicitly suppress zero-modes of hermitian Wilson-Dirac operator  $H_W = \gamma_5 D_W$  in order to avoid discontinuity of the overlap-Dirac operator  $D_{ov} = m_0(1 - \gamma_5 \cdot \text{sgn}(H_W(-m_0)))$  by introducing extra Wilson fermions which are irrelevant in the continuum [5]. As a result, the topological charge of our gauge configurations is fixed. We have chosen the trivial topological sector  $Q_{top} = 0$ .

In Section 2, we present the spectrum calculation focusing on new techniques using eigenmodes of the dirac operator. After making corrections to our data due to the finite size effects (FSE) in Section 3, we carry out chiral extrapolation of the corrected results using the NNLO ChPT formulae and compare the results with phenomenological values.

## 2. Spectrum calculation

In advance of the spectrum calculation, we compute and store 50 pairs of the lowest-lying eigenmodes of  $D_{ov}$  on each gauge configuration. With these data, we decompose the quark propagator as

$$S_q(x|y)_{\alpha\beta} = \sum_{i=-50}^{50} \frac{u_{\alpha}^i(x) \cdot u_{\beta}^i(y)}{\lambda_i + m_q^0} + S_q^{\text{high}}(x|y)_{\alpha\beta}, \quad (2.1)$$

where the indices  $\alpha, \beta$  represent spin $\times$ color and  $i$  labels eigenmode.  $m_q^0$  is the bare quark mass. While we use the conventional CG algorithm to obtain the second term with the source vector with low mode contributions projected out, we construct the first term from the eigenvalue  $\lambda_i$  and eigenvectors  $u_{\alpha}^i(x)$ . Since it is the low mode contribution which is computationally dominating the CG iteration,  $S_q^{\text{high}}$  can be obtained with much lower computational cost ( $\times 8$  less).

Computation of the meson correlator is done on 500 configurations separated by 20 HMC trajectories. When decomposing quark propagator as in (2.1), a part of the meson correlator is composed purely from the low mode contribution. By replacing this part by its average over the source location (low-mode-averaging [7, 8]), we can improve the data. Its advantage is apparent in Figure 1 where the effective mass of pseudo-scalar correlation functions with (filled symbols) and without (open symbols) low-mode-averaging are compared.

We obtain pion mass and decay constant from the pseudo-scalar correlators with smeared source and with local source. By fitting them simultaneously with single exponential functions sharing the same mass, we obtain the matrix element of the local operator  $|\langle 0|P|\pi\rangle|^2$ , from which  $f_{\pi}$  is computed, with a better statistical quality than solely using the local-local correlator.  $f_{\pi}$  is

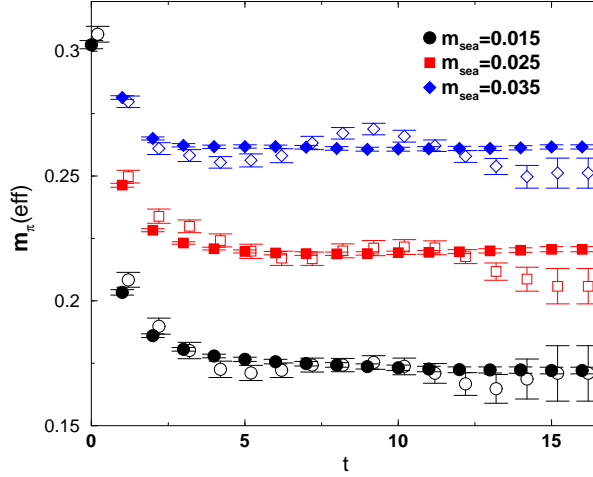


**Figure 1:** Effective mass from the P-P correlation function with smeared source for the lightest three quark masses  $m_{\text{sea}} = m_{\text{val}}$ . Open symbols represent data from conventional correlation function while filled ones are from low-mode-averaged correlator.

obtained though the axial Ward-Takahashi identity

$$f_\pi = 2m_q^0 \langle 0 | P | \pi \rangle / m_\pi^2, \quad (2.2)$$

without further renormalization. Note that we are using the  $f_\pi = 130$  MeV normalization.

Throughout this calculation, we use  $r_0 = 0.49$  fm as an input. Our lattice scale at the chiral limit is

$$a = 0.1184(12)(11) \text{ fm}. \quad (2.3)$$

By using its central value  $a^{-1} = 1.67$  GeV, the pion mass data points are in  $290 \text{ MeV} \leq m_\pi \leq 750$  MeV. Our heaviest  $m_q^0$  is roughly corresponding to the strange quark mass  $m_s$ .

We are interested in the chiral extrapolation of  $m_\pi^2/m_q$  and  $f_\pi$ , where  $m_q$  is the quark mass renormalized by the renormalization factor

$$Z_m^{\overline{\text{MS}}}(2 \text{ GeV}) = 0.742(12), \quad (2.4)$$

which is obtained non-perturbatively through the RI/MOM scheme on the lattice [9].

### 3. Finite size corrections

#### 3.1 Standard FSE

Some of our data points are in the region  $m_\pi L < 3.0$  where finite size effect could be significant. Therefore, it is important to estimate the correction to our data. To this end, we use the result of analytic calculation by Colangelo *et al.* [10]. Developing from the Lüscher's formula [11], which relates the mass-shift in a finite box to the amplitude of scattering of pions, they calculated the

finite volume corrections for  $m_\pi$  and  $f_\pi$ . Though their calculation includes NNNLO of ChPT for  $m_\pi$  and NNLO for  $f_\pi$ , we apply their NNLO results for both quantities. The NNLO effects depend on the low energy constants (LECs)  $\bar{l}_{1,2,3,4}$  of the  $N_f = 2$  ChPT. At the scale of the physical pion mass  $m_\pi^{\text{phys}} = 139.6$  MeV, they are estimated [12] as

$$\bar{l}_1^{\text{phys}} = -0.4 \pm 0.6, \quad (3.1)$$

$$\bar{l}_2^{\text{phys}} = 4.3 \pm 0.1, \quad (3.2)$$

$$\bar{l}_3^{\text{phys}} = 2.9 \pm 2.4, \quad (3.3)$$

$$\bar{l}_4^{\text{phys}} = 4.4 \pm 0.2. \quad (3.4)$$

We use these phenomenological values to correct our data. The errors in (3.1)–(3.4) are reflected in the results assuming a gaussian distribution. Because the Lüscher's formula is based on the full theory, we can use this result only for the data with the same mass for valence and sea quarks.

### 3.2 Correction for fixed $Q_{\text{top}}$

Since our numerical simulation is done at the topological charge fixed to zero, our observables are not free from the artifact. However, for large enough volume, local quantities such as hadron mass or matrix elements do not depend on  $Q_{\text{top}}$ . In fact it is verified by a saddle-point expansion [13] that the difference between the correlation function at fixed topological charge and that in the  $\theta$ -vacuum is of  $\mathcal{O}(V^{-1})$ . By using this relation to pion mass and decay constant, it can be shown that the leading correction is proportional to their second derivative with respect to  $\theta$  dependence at the saddle point  $\theta_s = iQ_{\text{top}}/(V\chi_t)$ .  $\chi_t$  is the topological susceptibility, which is calculated on the same set of configurations [14]. At NLO of ChPT we obtain the corrections

$$\frac{m_\pi^{Q_{\text{top}}=0}}{m_\pi(\theta=0)} = 1 - \frac{1}{16V\chi_t} \left[ 1 + \left( \frac{m_\pi^{\text{tree}}(\theta=0)}{4\pi f} \right)^2 \left( \ln \left( \frac{m_\pi^{\text{tree}}(\theta=0)}{m_\pi^{\text{phys}}} \right)^2 - \bar{l}_3^{\text{phys}} + 1 \right) \right], \quad (3.5)$$

$$\frac{f_\pi^{Q_{\text{top}}=0}}{f_\pi(\theta=0)} = 1 + \frac{1}{4V\chi_t} \left( \frac{m_\pi^{\text{tree}}(\theta=0)}{4\pi f} \right)^2 \left( \ln \left( \frac{m_\pi^{\text{tree}}(\theta=0)}{m_\pi^{\text{phys}}} \right)^2 - \bar{l}_4^{\text{phys}} + 1 \right), \quad (3.6)$$

where  $m_\pi^{\text{tree}}(\theta)^2 = 2B_0m_q \cos(\theta/N_f)$  is the tree-level  $\theta$ -dependent pion mass. The fixed  $Q_{\text{top}}$  correction starts at the tree-level for  $m_\pi$  while it does at NLO for  $f_\pi$ .

In Figure 2, we illustrate the effects of finite size effects for  $m_\pi^2/m_q$  (left) and  $f_\pi$  (right). In each panel, the original data (black diamonds) are corrected by the standard FSE (blue squares) and further by the fixed topology effect (red circles). For the data with the lightest quark mass, the standard FSE is 4.5 % and 6.0 % for  $m_\pi^2/m_q$  and  $f_\pi$ , respectively. For  $m_\pi^2/m_q$  in small mass region, two finite size effects appear with an opposite sign to almost cancel each other.

## 4. Chiral extrapolation

While conventional  $N_f = 2$  full ChPT expansion formulae are written in power of  $(m_\pi^2)^{\text{tree}} = 2B_0m_q$ , we chose  $\xi = (m_\pi/(4\pi f_\pi))^2$  as an expansion parameter. This choice enables us to fit the

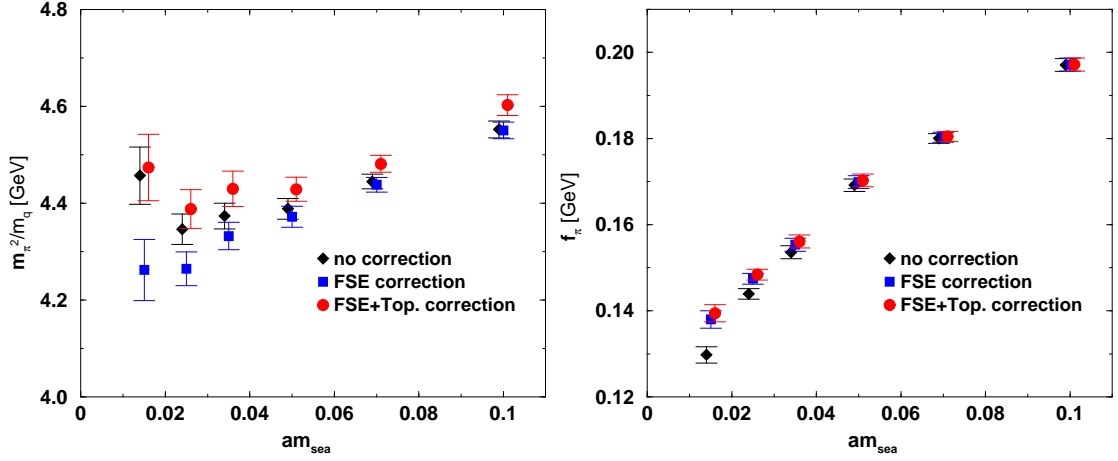


**Figure 2:** Results of finite size corrections for  $m_\pi^2/m_q$  (left) and  $f_\pi$  (right). Data points as a function of  $m_{\text{sea}}$  are slightly shifted for visibility.

ChPT formulae (almost) independently to  $m_\pi^2/m_q$  and  $f_\pi$  as a function of  $\xi$  which is a measurable quantity at each quark mass. The NLO formulae are

$$(m_\pi^2/m_q)_{\text{NLO}} = 2B_0 (1 + \xi \ln \xi - \bar{l}_3 \xi), \quad (4.1)$$

$$(f_\pi)_{\text{NLO}} = f (1 - 2\xi \ln \xi + 2\bar{l}_4 \xi) \quad (4.2)$$

where  $\bar{l}_{3,4}$ ,  $B_0$  and  $f$  are to be fitted.  $\bar{l}_{3,4}$  are LECs at the scale  $4\pi f$ . Since these two formulae do not share any fit parameter, independent fits are possible.

We also examine the NNLO formulae which are written as

$$(m_\pi^2/m_q)_{\text{NNLO}} = 2B_0 \left[ 1 + \xi \ln \xi + \frac{7}{2}(\xi \ln \xi)^2 - \bar{l}_3(\xi - 9\xi^2 \ln \xi) + \left( \bar{l}_4 - \frac{4}{3}(\tilde{l}^{\text{phys}} + 16) \right) \xi^2 \ln \xi \right] + \alpha_1 \xi^2 + \mathcal{O}(\xi^3), \quad (4.3)$$

$$(f_\pi)_{\text{NNLO}} = f \left[ 1 - 2\xi \ln \xi + 5(\xi \ln \xi)^2 + 2\bar{l}_4(\xi - 10\xi^2 \ln \xi) + \frac{3}{2} \left( \tilde{l}^{\text{phys}} + \frac{53}{2} \right) \xi^2 \ln \xi \right] + \alpha_2 \xi^2 + \mathcal{O}(\xi^3), \quad (4.4)$$

where coefficients of the  $\xi^2$  term  $\alpha_1$  and  $\alpha_2$  contain unknown low energy constants associated with the NNLO counterterms. In carrying out the chiral fit with these formulae, an input

$$\tilde{l}^{\text{phys}} \equiv 7\bar{l}_1^{\text{phys}} + 8\bar{l}_2^{\text{phys}} - 15 \ln \left( \frac{4\pi f_\pi^{\text{phys}}}{m_\pi^{\text{phys}}} \right)^2 \quad (4.5)$$

is introduced from phenomenological estimates (3.1) and (3.2) with  $f_\pi^{\text{phys}} = 130.0$  MeV.

In our target range  $0 < \xi \lesssim 0.1$ , an approximation  $\xi^2 \ln \xi \approx -2.5\xi^2$  is numerically rather precise. Therefore, it is reasonable to consider yet another fit ansatz with modified NNLO formulae,

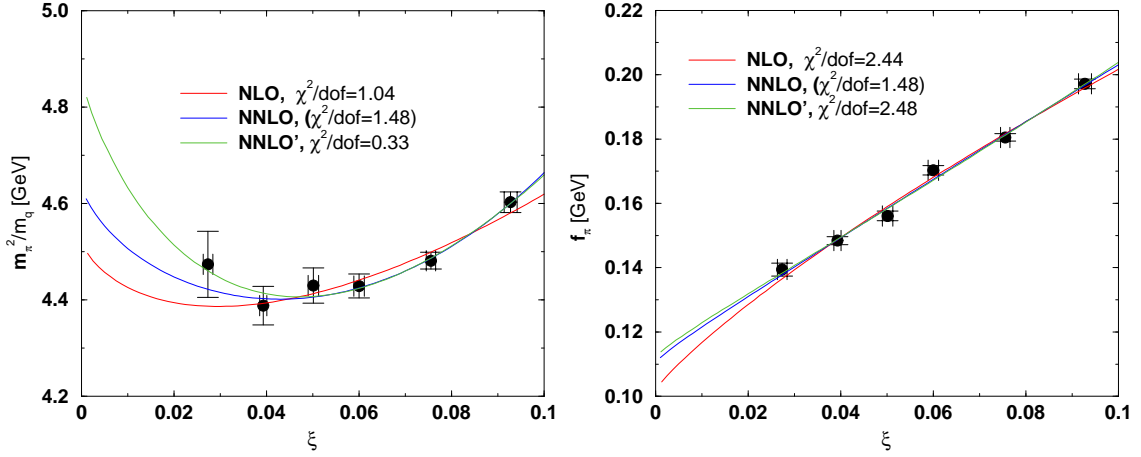


**Figure 3:** Results of chiral extrapolation for  $m_\pi^2/m_q$  [GeV] (left) and  $f_\pi$  [GeV] (right) as a function of  $\xi$ . For each panel, three kinds of fit (NLO, NNLO and NNLO') by using all data points are shown.

which we call NNLO'

$$(m_\pi^2/m_q)_{\text{NNLO}'} = 2B_0 \left[ 1 + \xi \ln \xi + \frac{7}{2} (\xi \ln \xi)^2 - \bar{l}_3 \xi \right] + \alpha'_1 \xi^2 + \mathcal{O}(\xi^3), \quad (4.6)$$

$$(f_\pi)_{\text{NNLO}'} = f \left[ 1 - 2\xi \ln \xi + 5(\xi \ln \xi)^2 + 2\bar{l}_4 \xi \right] + \alpha'_2 \xi^2 + \mathcal{O}(\xi^3). \quad (4.7)$$

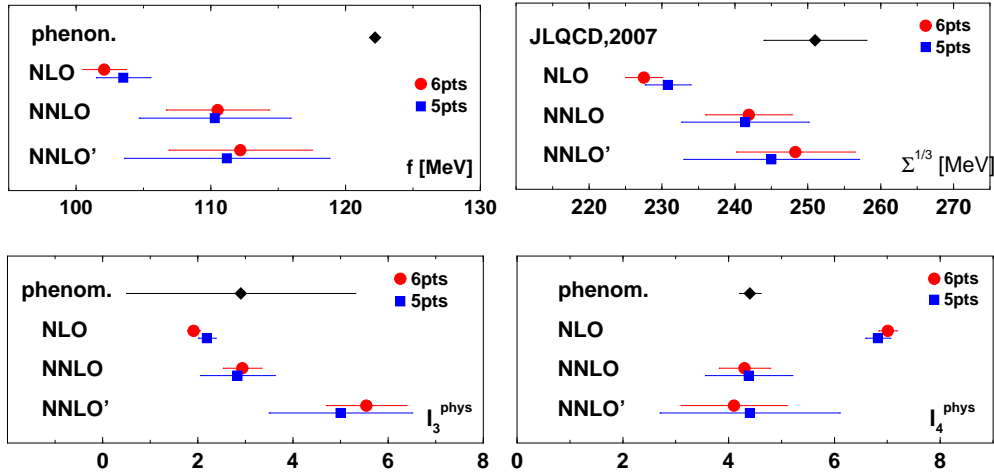
In Figure 3 we show the results of chiral fits to the FSE corrected data of  $m_\pi^2/m_q$  and  $f_\pi$ , respectively. In each panel, we compare NLO (red curves), NNLO (blue) and NNLO' (green). Note that we cannot compare the quality of the fit with NNLO and others by the values of  $\chi^2/\text{dof}$  because we carry out the simultaneous fit for the former and independent fits for the latter.

Figure 4 compares quantities from our fit:  $f$ ,  $\Sigma = B_0 \cdot f^2/2$ ,  $\bar{l}_3^{\text{phys}}$  and  $\bar{l}_4^{\text{phys}}$ . In the figure we also plot phenomenological values of  $f$  [15] and  $\bar{l}_{3,4}^{\text{phys}}$  ((3.3) and (3.4)) as well as the result of our previous calculation in  $\varepsilon$ -regime [16]:  $\Sigma^{1/3} = 0.251(7)(11)$  GeV.

We see that, for  $\bar{l}_3^{\text{phys}}$ , large error of the phenomenological estimate covers all of our results. For other quantities, results from NLO fit are inconsistent with the NNLO results. This implies the failure of the NLO formulae to describe the data in the quark mass region up to  $m_s$ . Results from NNLO and NNLO' are consistent with each other and with phenomenological estimates.

For the future we are planning to extend the present analysis to  $m_K$  and  $f_K$  on the  $N_f = 2 + 1$  dynamical lattices (see [17] for the status). Numerical check of the estimate of FSE in a bigger volume is also planned.

Numerical simulations are performed on Hitachi SR11000 and IBM System Blue Gene Solution at High Energy Accelerator Research Organization (KEK) under a support of its Large Scale Simulation Program (No. 07-16). This work is supported in part by the Grant-in-Aid of the Ministry of Education (Nos. 13135204, 15540251, 17740171, 18034011, 18340075, 18740167, 18840045, 19540286, 19740121, 19740160).



these reference points.

**Figure 4:** Comparison of physical quantities obtained from chiral fit ansatz:  $f$  (upper left),  $\Sigma^{1/3}$  (upper right),  $l_3^{\text{phys}}$  (lower left) and  $l_4^{\text{phys}}$  (lower right). In each panel, red circles and blue squares are corresponding to fits with 6 and 5 lightest data points, respectively.

## References

- [1] H. Neuberger, Phys. Lett. **B427** (1998) 353 [arXiv:hep-lat/9801031].
- [2] H. Matsufuru *et al.* (JLQCD Collaboration), PoS LAT 2006:031 [arXiv:hep-lat/0610026].
- [3] S. Hashimoto *et al.* (JLQCD Collaboration), PoS LAT 2006:052 [arXiv:hep-lat/0610011].
- [4] T. Kaneko *et al.* (JLQCD Collaboration), PoS LAT 2006:054 [arXiv:hep-lat/0610036].
- [5] H. Fukaya *et al.* (JLQCD Collaboration), Phys. Rev. D **74** (2006) 094505.
- [6] H. Matsufuru, in these proceedings, PoS LAT 2007:018.
- [7] T. DeGrand and S. Schaefer, Comp. Phys. Comm. **159** (2004) 185.
- [8] L. Giusti, P. Hernández, M. Laine, P. Weisz, H. Wittig, JHEP **04** (2004) 013.
- [9] G. Martinelli, C. Pittori, C. T. Sachrajda, M. Testa and A. Vladikaa, Nucl. Phys. **B445** (1995) 81.
- [10] G. Colangelo, S. Dürr and C. Haefeli, Nucl. Phys. **B721** (2005) 136.
- [11] M. Lüscher, Commun. Math. Phys. **104** (1986) 177.
- [12] G. Colangelo, J. Gasser and H. Leutwyler, Nucl. Phys. **B603** (2001) 125.
- [13] R. Brower, S. Chandrasekharan, J. W. Negele and U.-J. Wiese, Phys. Lett. **B560** (2003) 64.
- [14] Ting-Wai Chiu, in these proceedings; S. Aoki *et al.* (JLQCD-TWQCD Collaborations), in preparation.
- [15] J. Gasser and H. Leutwyler, Ann. of Phys. **158** (1984) 142.
- [16] H. Fukaya *et al.* (JLQCD-TWQCD Collaborations), Phys. Rev. Lett. **98** (2007) 172001; Phys. Rev. D **76** (2007) 054503.
- [17] JLQCD Collaboration (S. Hashimoto *et al.*), in these proceedings, PoS LAT 2007:101.